The Astrophysical Journal, 696:L106–L109, 2009 May 1 doi:10.1088/0004-637X/696/1/L106

MEASUREMENTS OF ABSORPTION, EMISSIVITY REDUCTION, AND LOCAL SUPPRESSION OF SOLAR ACOUSTIC WAVES IN SUNSPOTS

Dean-Yi Chou[1], Zhi-Chao Liang[1], Ming-Hsu Yang[1], Hui Zhao[1], and Ming-Tsung Sun[2]
[1] Physics Department, National Tsing Hua University, Hsinchu, Taiwan; chou@phys.nthu.edu.tw
[2] Department of Mechanical Engineering, Chang-Gung University, Kwei-San, Taiwan
Received 2009 March 2; accepted 2009 March 30; published 2009 April 16

ABSTRACT

The power of solar acoustic waves in magnetic regions is lower relative to the quiet Sun. Absorption, emissivity reduction, and local suppression of acoustic waves contribute to the observed power reduction in magnetic regions. We propose a model for the energy budget of acoustic waves propagating through a sunspot in terms of the coefficients of absorption, emissivity reduction, and local suppression of the sunspot. Using the property that the waves emitted along the wave path between two points have no correlation with the signal at the starting point, we can separate the effects of these three mechanisms. Applying this method to helioseismic data filtered with direction and phase-velocity filters, we measure the fraction of the contribution of each mechanism to the power deficit in the umbra of the leading sunspot of NOAA 9057. The contribution from absorption is $23.3 \pm 1.3\%$, emissivity reduction $8.2 \pm 1.4\%$, and local suppression $68.5 \pm 1.5\%$, for a wave packet corresponding to a phase velocity of 6.98×10^{-5} rad s^{-1}.

Key words: Sun: activity – Sun: helioseismology – Sun: interior – sunspots

1. INTRODUCTION

Observations show that the power of solar acoustic waves is reduced in magnetic regions. The mechanisms causing the power reduction in magnetic regions are divided into three categories: absorption, emissivity reduction, and local suppression (Hollweg 1988; Cally & Bogdan 1993; Hindman et al. 1997; Crouch & Cally 2005; Wachter et al. 2006; Parchevsky & Kosovichev 2007; Rajaguru et al. 2007; Gordovskyy & Jain 2008; Chou et al. 2009a, 2009b). All three mechanisms contribute to the power directly measured in acoustic-power maps (Lites et al. 1982; Braun et al. 1992; Hindman & Brown 1998; Ladenkov et al. 2002), while only absorption and emissivity reduction contribute to the measurements in Hankel analysis (Braun et al. 1987; Bogdan et al. 1993; Braun 1995; Chen et al. 1996). Determining the contribution from these three mechanisms in sunspots is one of the important problems in local helioseismology. Chou et al. (2009a, hereinafter called Paper I) have used the property that the waves emitted along the wave path between two points have no correlation with the signal at the starting point to separate the effects of absorption from those of emissivity reduction and local suppression. The absorption coefficient has been defined and measured in Paper I. In this study, we go one step further to define and measure the coefficients of emissivity reduction and local suppression.

2. METHOD

A model for the energy budget of acoustic waves propagating through the quiet Sun and a sunspot is illustrated with schematic diagrams in Figure 1. The upper diagram shows the energy budget in the quiet Sun. A wave packet, formed by modes with similar horizontal phase velocity, propagating in a particular horizontal direction, has a ray path shown in Figure 1. The power in the quiet Sun is uniform with a value I. As the wave packet propagates from A to B, its power is reduced to $(1-d)I$ owing to dissipation, where d is the dissipation coefficient in the quiet Sun. Energy generated along the path is eI, where e is the emission coefficient in the quiet Sun. The uniformity of power in the quiet Sun leads to $e = d$. As the wave packet propagates from B to C, the power at B is reduced further by a factor of $(1-d)$. On the way from B to C, power eI is generated again. The total power at C equals to I as expected. It is noted that d and e represent the dissipation and emission, respectively, as the wave packet travels the one-skip distance in the quiet Sun.

If a sunspot is present at B, the energy budget is shown in the lower diagram of Figure 1. The acoustic power at B could be reduced by absorption, emissivity reduction, and local suppression. As the wave packet propagates from A to B, besides the dissipation in the quiet Sun, the power coming from A and arriving at B is reduced by a factor of $(1-a)$ owing to the absorption in the sunspot, where a is the absorption coefficient. Energy generated along the path from A to B is reduced by a factor of $(1-r)$ owing to the magnetic field in the sunspot, where r is the emissivity reduction coefficient. Both $(1-a)(1-d)I$ and $(1-r)eI$ are reduced by a factor of $(1-s)$ because of local suppression in the sunspot, where s is the local suppression coefficient. Only part of the power at B, $(1-s)(1-a)(1-d)I$, correlates with that at A. The power $(1-s)(1-r)eI$ at B, generated along the path between A and B, has no correlation with that at A.

As the wave packet propagates from B to C, its power is reduced further by a factor of $(1-a)(1-d)$, but local suppression disappears at C because it is located outside the sunspot. Energy generated on the way from B to C is again $(1-r)eI$. It is noted that the coefficients a and r defined here account for only the contribution from half the wave path inside the sunspot. The contribution from the first half of the path (propagating upward) and the second half (propagating downward) may be different, depending on the location of B in the sunspot. That is, the value of a and r for the path from A to B may be different from that from B to C. For simplicity, we assume that a and r are the same for the upward and downward paths. This is a reasonable approximation if a and r are averaged over an area in the sunspot, as done in our analysis.

For the powers at A, B, and C, only those connected by the arrows shown in Figure 1 correlate. In Paper I, the correlation between A and C is used to determine the value of a. The

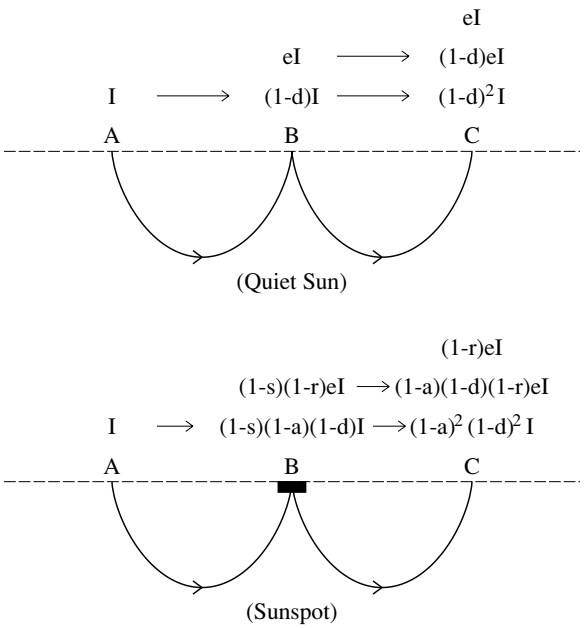

Figure 1. Schematic plot for energy budget of solar acoustic waves propagating in one horizontal direction (see the text for explanation).

cross-correlation function (CCF) between A and C is computed as

$$F_{AC}(\tau) = \frac{\sum_t \Psi_A(t)\Psi_C(t+\tau)}{\sum_t [\Psi_A(t)]^2} \quad (1)$$

where Ψ_A and Ψ_C are the wave functions (velocity fields) at A and C, respectively. It is noted that the normalization factor defined here is the sum of the square of the wave function at A over time, different from the conventional definition. The CCF $F_{AC}(\tau)$ corresponds to the second skip for our wave packet. The magnitude of $F_{AC}(\tau)$, hereinafter denoted by F_{AC}, is the peak value of the envelope of $F_{AC}(\tau)$. The width of the CCF increases with the number of skips owing to the dispersion of the wave packet, but the product of the square of the magnitude of the CCF and the width remains unchanged in the absence of dissipation and absorption (Chou & Ladenkov 2007; Burtseva et al. 2007). To correct the effect of dispersion, we compute the width-corrected CCF, $\tilde{F}_{AC} \equiv F_{AC}(W_{AC})^{1/2}$, where W_{AC} is the ratio of the width of the CCF at C to that at A. The CCF at A is simply the autocorrelation function at A. Note that W_{AC} defined here is different from that in Paper I. The width-corrected CCF, $\tilde{F}_{AC}$, is proportional to the square root of the power at C that correlates with the signal at A. For the quiet Sun,

$$1 - d = \tilde{F}_{AC}^{(\mathrm{qs})}. \quad (2)$$

For the sunspot, $\tilde{F}_{AC}^{(\mathrm{sp})} = (1-a)(1-d)$. Thus, $(1-a)$ can be expressed as

$$1 - a = \frac{\tilde{F}_{AC}^{(\mathrm{sp})}}{\tilde{F}_{AC}^{(\mathrm{qs})}}. \quad (3)$$

This formula has been used in Paper I to determine the value of a for a sunspot in NOAA 9062.

Similarly, one can compute the CCF between A and B that yields $\tilde{F}_{AB}^{(\mathrm{sp})} = [(1-s)(1-a)(1-d)]^{1/2}$ if $\sum_t |\Psi_A(t)|^2$ is the normalization constant like Equation (1). Thus, $(1-s)$ can be expressed as

$$1 - s = \frac{[\tilde{F}_{AB}^{(\mathrm{sp})}]^2}{\tilde{F}_{AC}^{(\mathrm{sp})}}. \quad (4)$$

The last coefficient to be determined is r that relates to the CCF between B and C. From Figure 1, the power $(1-s)(1-a)(1-d)I$ at B correlates with the power $(1-a)^2(1-d)^2 I$ at C, and the power $(1-s)(1-r)eI$ at B correlates with the power $(1-a)(1-d)(1-r)eI$ at C. If we use $\sum_t |\Psi_A(t)|^2$ as the normalization constant in computing the CCF between B and C, $\tilde{F}_{BC}^{(\mathrm{sp})} = [(1-s)(1-a)(1-d)]^{1/2}[(1-a)(1-d)+(1-r)d]$. Together with Equations (2), (3), and (4), $(1-r)$ can be expressed as

$$1 - r = \left[\frac{\tilde{F}_{BC}^{(\mathrm{sp})}}{\tilde{F}_{AB}^{(\mathrm{sp})}} - \tilde{F}_{AC}^{(\mathrm{sp})}\right]\left[1 - \tilde{F}_{AC}^{(\mathrm{qs})}\right]^{-1}. \quad (5)$$

3. DATA AND ANALYSIS

In this study, we use the helioseismic data taken with MDI onboard the *Solar and Heliospheric Observatory* (Scherrer et al. 1995). The data are 1024 × 1024 full-disk Dopplergrams taken at a rate of one image per minute. A time series of 2048 minutes taken in a period of 2000 June 29–30 is used in this study. The procedure of the preliminary data reduction is similar to that in Paper I and Chou et al. (2009b). It is briefly described as follows. (1) The 61-frame running mean is subtracted from the measured signal at each spatial point. (2) A temporal filter is applied to remove signals below 1.5 mHz and above 5.0 mHz. (3) Each full-disk image is transformed into coordinates of longitude and latitude. (4) The differential rotation of the solar surface is removed. (5) An area centered at the leading sunspot of NOAA 9057 is selected, and each image is transformed into a coordinate system of (ϕ, θ), centered at the sunspot center, where ϕ is the east–west direction and θ the north–south direction. The dimension of the selected region is 30° in ϕ and 30° in θ, corresponding to 256 × 256 pixels.

The waves above the cutoff frequency escape into the outer atmosphere, and would complicate the interpretation of the measured CCFs. Thus, we apply a filter to remove the waves above 5 mHz to avoid the complication.

The data cube after the above procedure is ready for further analysis. The acoustic-power map of the selected area is shown in Figure 2(b). The corresponding magnetic map is shown in Figure 2(a). A direction filter and a phase-velocity filter are applied to isolate waves propagating in a narrow range of directions and phase velocities. The details of direction filters and phase-velocity filters have been discussed in Chou et al. (2009b). The direction filters used in this study are either northward or southward, with three different widths: 10°, 15°, and 20°. The phase-velocity filter used in this study is centered at 6.98×10^{-5} rad s^{-1} (corresponding to $\ell = 300$ at 3.33 mHz) with a width of 5.82×10^{-5} rad s^{-1}. Both direction and phase-velocity filters are smoothed by a Hanning window. Two examples of acoustic-power map filtered with direction and phase-velocity filters are shown in Figures 2(c) and (d).

In Figures 2(c) and (d), a secondary image appears behind the leading sunspot with respect to the wave direction. The separation between the secondary image and the sunspot is consistent with the one-skip travel distance associated with the phase-velocity filter. In the following discussion, points B and C in Figure 1 are placed at the locations of the sunspot and the secondary image, respectively. Point A is located at the opposite side of the secondary image. The CCF using A as the reference

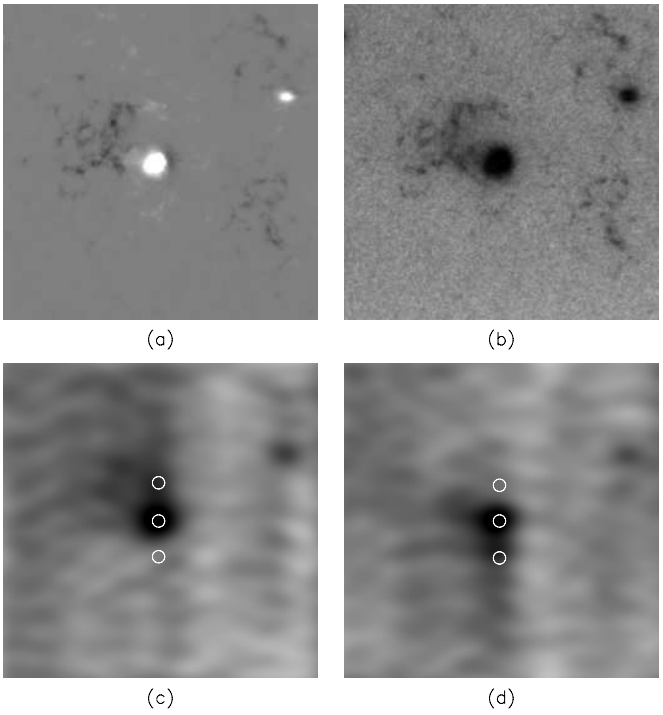

Figure 2. (a) Magnetic map, (b) raw acoustic-power map, (c) acoustic-power map of the waves filtered with the northward direction and phase-velocity filters; (d) acoustic-power map of the waves filtered with the southward direction and phase-velocity filters. The width of the direction filter is 15°. The phase-velocity filter is described in the text. The white circles indicate the areas of *A*, *B*, and *C*.

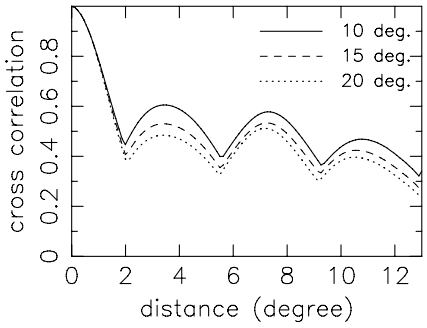

Figure 3. Peak value of the envelope of cross-correlation function vs. angular distance for the southward waves filtered with direction filter of three different widths.

point is computed. The computation of CCF is repeated for different reference points in a circular area with a radius of 5 pixels such that point *B* is located inside the umbra. (The radius of the umbra is about 5 pixels.) The areas of *A*, *B*, and *C* are indicated by the white circles in Figures 2(c) and (d). These CCFs are averaged to reduce noise. The envelope of the average CCF at each distance is determined by a method of demodulation (Bracewell 1986). The peak value of the envelope vs. distance is shown in Figure 3. The first peak in Figure 3, corresponding to the first skip, is the magnitude of the CCF between *A* and *B*, $F_{AB}^{(\mathrm{sp})}$. The second peak, corresponding to the second skip, is the magnitude of the CCF between *A* and *C*, $F_{AC}^{(\mathrm{sp})}$. To correct the effect of dispersion, we need to determine the width (FWHM) of the CCF at *A*, *B*, and *C*. The width-corrected magnitude $\tilde{F}_{AB}^{(\mathrm{sp})} = F_{AB}^{(\mathrm{sp})}[W_{AB}^{(\mathrm{sp})}]^{1/2}$ and $\tilde{F}_{AC}^{(\mathrm{sp})} = F_{AC}^{(\mathrm{sp})}[W_{AC}^{(\mathrm{sp})}]^{1/2}$, as described in Section 2. Similarly, we also compute the CCF between *B* and *C* to determine $\tilde{F}_{BC}^{(\mathrm{sp})}$.

Table 1
Measured Parameters

Parameter	N10°	N15°	N20°	S10°	S15°	S20°
d	0.252	0.256	0.269	0.279	0.282	0.293
a	0.182	0.204	0.235	0.116	0.165	0.188
s	0.383	0.510	0.583	0.355	0.474	0.546
r	0.146	0.243	0.245	0.080	0.153	0.191
P_B	0.511	0.385	0.318	0.576	0.441	0.368
P'_B	0.530	0.410	0.337	0.592	0.462	0.387
P_C	0.722	0.659	0.630	0.826	0.741	0.702
P'_C	0.731	0.673	0.637	0.864	0.756	0.703
$\tilde{a}$	0.278	0.247	0.252	0.197	0.212	0.211
$\tilde{s}$	0.647	0.652	0.652	0.750	0.710	0.700
$\tilde{r}$	0.075	0.101	0.097	0.053	0.077	0.089

The same procedure can be carried out for the quiet Sun to obtain $\tilde{F}_{AC}^{(\mathrm{qs})}$. In this study, we use an area of $30^\circ \times 30^\circ$ in the quiet Sun to compute $\tilde{F}_{AC}^{(\mathrm{qs})}$. Using four width-corrected magnitudes $\tilde{F}_{AC}^{(\mathrm{qs})}$, $\tilde{F}_{AB}^{(\mathrm{sp})}$, $\tilde{F}_{AC}^{(\mathrm{sp})}$, and $\tilde{F}_{BC}^{(\mathrm{sp})}$, together with Equations (2), (3), (4), and (5), we can compute the four coefficients *d*, *a*, *s*, and *r*. The results of *d*, *a*, *s*, and *r* for different directions and widths are shown in Table 1.

4. DISCUSSION

From Figure 1, the total power at *B*, in units of *I*, is $P_B = (1-s)(1-a)(1-d)+(1-s)(1-r)d$. The total power at *C* is $P_C = (1-a)^2(1-d)^2+(1-a)(1-d)(1-r)d+(1-r)d$. The values of P_B and P_C computed with *d*, *a*, *s*, and *r* are shown in Table 1. We can also directly measure the power at *B* and *C*, in units of power at *A*, from the acoustic-power map. The measured power averaged over a circular area with a radius of 5 pixels in the umbra, denoted by P'_B, and in the secondary image, denoted by P'_C, is shown in Table 1. The difference between P_B and P'_B or between P_C and P'_C is less than 7%. It is noted that they are computed with totally different methods: P_B and P_C are computed with the CCFs at *A*, *B*, and *C*, while P'_B and P'_C are purely local and computed directly from the acoustic-power map. The consistency between the values derived from two different methods supports two things: the model of energy budget described in Figure 1, and the values of *a*, *s*, and *r* determined with our method. We have tested the consistency between P_B and P'_B or between P_C and P'_C for different energy budget models with some modifications to the model in Figure 1. These modified models do not yield the consistency.

Table 1 shows that all of three coefficients *a*, *s*, and *r* increase with the width of direction filter for both northward and southward waves. This phenomenon connects with the increase in the power deficit in the sunspot, $(1-P_B)$ or $(1-P'_B)$, and the power deficit in the secondary image, $(1-P_C)$ or $(1-P'_C)$, with width. This can be understood with the complementary property between the spatial domain and the corresponding Fourier domain: signals filtered with the direction filter spread in the direction perpendicular to the wave direction; the narrower the direction filter, the more spreading the signals (Chou et al. 2009b). Thus the power deficit in the sunspot is smaller for a narrower direction filter. This also leads to smaller *a*, *s*, and *r* for a narrower direction filter. Since their values depend on the width of the direction filter used in analysis, the coefficients *a*, *s*, and *r* measured with our method are not appropriate parameters to represent the three mechanisms: absorption, local suppression, and emissivity reduction, respectively. A better parameter for each mechanism is the fraction of the contribution

Table 2
Averaged Parameters

Parameter	N	S	Average of N and S
Average $\tilde{a}$	0.259 ± 0.017	0.207 ± 0.008	0.233 ± 0.013
Average $\tilde{s}$	0.650 ± 0.003	0.720 ± 0.026	0.685 ± 0.015
Average $\tilde{r}$	0.091 ± 0.009	0.073 ± 0.018	0.082 ± 0.014

of the mechanism to the power deficit in the sunspot, hereinafter called the normalized coefficient. From Figure 1, the fraction of contribution of absorption to the power deficit in the sunspot is $\tilde{a} = a(1-d)(1-P_B)^{-1}$. Its value is listed in Table 1. The discrepancy in $\tilde{a}$ among different widths significantly reduces, and unlike a, $\tilde{a}$ no longer depends on the width. Similarly, the fraction of the contribution of emissivity reduction to the power deficit in the sunspot is $\tilde{r} = rd(1-P_B)^{-1}$. The fraction of the contribution of local suppression to the power deficit in the sunspot is $\tilde{s} = s[(1-a)(1-d)+(1-r)d](1-P_B)^{-1} = [s(1-s)^{-1}][P_B(1-P_B)^{-1}]$. The values of $\tilde{r}$ and $\tilde{s}$ are also listed in Table 1. Like $\tilde{a}$, the discrepancy among different widths for $\tilde{s}$ and $\tilde{r}$ significantly reduces, and no longer depends on the width. It can be shown that $\tilde{a}+\tilde{s}+\tilde{r}=1$.

If we adopt the variations of each normalized coefficient among different widths as measurement errors, we can compute the mean value averaged over different widths and the error. The results are shown in Table 2. The difference between the values determined from the northward and southward waves could be caused by the asymmetric distribution of the magnetic field in and around the sunspot. The last column in Table 2 is the average of the northward and southward values.

It should be noted that the coefficients determined here are associated with a specific wave packet. The dependence on frequency and phase velocity could provide more complete information on the interaction between the acoustic waves and the sunspot. It is also of interest to study variations of three coefficients with wave direction.

The surface flows in and around sunspots would modify the local acoustic power: The local acoustic power would increase if the flows and waves have the same direction, and decrease if they have the opposite directions (Landau & Lifshitz 1987). This local change in acoustic power would appear as an effect of local suppression. Thus the flows in the sunspot would modify the coefficient of local suppression of the sunspot, while the flows at A and C would complicate the energy budget model because two additional coefficients of local suppression at A and C need to be introduced.

5. SUMMARY

We propose an energy budget model for the waves propagating through a sunspot as shown in Figure 1. The model contains four coefficients: d (dissipation in the quiet Sun), a (absorption), r (emissivity reduction), and s (local suppression). We use the property that the waves emitted along the wave path between two points have no correlation with the signal at the starting point to separate the effects of absorption, emissivity reduction, and local suppression in a sunspot. The coefficient d can be determined from the CCF in the quiet Sun. The coefficients a, r, and s can be determined from three CCFs between three points: A, B (sunspot), and C (secondary image). We apply this method to the leading sunspot of NOAA 9057. Although the value of a, r, and s depends on the width of direction filter, the normalized coefficients $\tilde{a}$, $\tilde{s}$, and $\tilde{r}$, defined as the fraction of the contribution of each mechanism to the power deficit in the sunspot, are independent of the width of direction filter. The powers in the sunspot and secondary image computed from a, r, and s are consistent with the powers directly measured in the sunspot and secondary image within 7%. This supports the model of energy budget proposed here and the values of a, r, and s measured with our method.

SOHO is a project of international cooperation between ESA and NASA. The authors are supported by the NSC of ROC under grant NSC-96-2112-M-007-034-MY3.

REFERENCES

Bracewell, R. N. 1986, The Fourier Transform and Its Applications (New York: McGraw-Hill)
Bogdan, T. J., Brown, T. B., Lites, B. W., & Thomas, J. H. 1993, ApJ, 406, 723
Braun, D. C. 1995, ApJ, 451, 859
Braun, D. C., Duvall, T. L., Jr., & LaBonte, B. J. 1987, ApJ, 319, L27
Braun, D. C., Lindsey, C., Fan, Y., & Jefferies, S. M. 1992, ApJ, 392, 739
Burtseva, O., Kholikov, S., Serebryanskiy, A., & Chou, D.-Y. 2007, Sol. Phys., 241, 17
Cally, P. S., & Bogdan, T. J. 1993, ApJ, 402, 721
Chen, K.-R., & Chou, D.-Y. the TON Team 1996, ApJ, 465, 985
Chou, D.-Y., & Ladenkov, O. 2007, Sol. Phys., 241, 7
Chou, D.-Y., Yang, M.-H., Liang, Z.-C., & Sun, M.-T. 2009a, ApJ, 690, L23 (Paper I)
Chou, D.-Y., Liang, Z.-C., Yang, M.-H., & Sun, M.-T. 2009b, Sol. Phys., 255, 39
Crouch, A. D., & Cally, P. S. 2005, Sol. Phys., 227, 1
Gordovskyy, M., & Jain, R. 2008, ApJ, 681, 664
Hindman, B. W., & Brown, T. M. 1998, ApJ, 504, 1029
Hindman, B. W., Jain, R., & Zweibel, E. G. 1997, ApJ, 476, 392
Hollweg, J. V. 1988, ApJ, 335, 1005
Ladenkov, O. V., Hill, F., Egamberdiev, S. A., & Chou, D.-Y. 2002, Astron. Lett., 28, 411
Landau, L. D., & Lifshitz, E. M. 1987, Fluid Mechanics (Oxford: Pergamon), section 68
Lites, B. W., White, O. R., & Packman, D. 1982, ApJ, 253, 386
Parchevsky, K. V., & Kosovichev, A. G. 2007, ApJ, 666, L53
Rajaguru, S. P., Sankarasubramanian, K., Wachter, R., & Scherrer, P. H. 2007, ApJ, 654, L178
Scherrer, P. H., et al. 1995, Sol. Phys., 160, 237
Wachter, R., Schou, J., & Sankarasubramanian, K. 2006, ApJ, 648, 1256